Transmitarray Antenna Based on Low-Profile Multi-resonance C-patch and C-slot Elements

Minh Thien Nguyen[1,2], Linh Mai[3,4], and Binh Duong Nguyen[1,2,*]

[1] School of Electrical Engineering, International University, Ho Chi Minh City, Vietnam
[2] Vietnam National University, Ho Chi Minh City, Vietnam
[3] Faculty of Electronics and Telecommunications, University of Engineering and Technology, Hanoi City, Vietnam
[4] Vietnam National University, Hanoi City, Vietnam
Email: nmthien@hcmiu.edu.vn (M.T.N.), linhmai@vnu.edu.vn (L.M.); nbduong@hcmiu.edu.vn (B.D.N.)
*Corresponding author

***Abstract*—Transmitarray unit-cells, typically multi-layered, have several design challenges. These structures require many thick substrates between layers. This makes the transmitarray costly and bulky. Besides, significant modifications of the size of radiating layers to achieve phase variation may lead to discrepancies between unit-cell performance in periodic boundary simulation and that in the real transmitarray. This paper proposes a 2-bit transmitarray unit-cell structure made from two substrates and a combination of C-patches and C-slots. Thanks to the multi-resonance characteristics of the C-patches and C-slots, a large phase shift can be primarily realized through varying the slot length of the C-slots on the middle layers. As a result, the radiating elements in the array are the same size. A low-cost, thin transmitarray prototype is fabricated and measured. Experimental results reveal a 1-dB bandwidth of 7%. A peak aperture efficiency is achieved of 43% at 11.8 GHz. Furthermore, the side lobe level is less than 18 dB, and cross-polarization radiation is below 30 dB.**

***Keywords*—cut-ring patch, cut-ring slot, reflectarray, transmitarray, unit-cell design**

I. Introduction

In order to create a high directivity antenna and beam steering, transmitarray antenna, which consists of a source antenna and an array of phase shifting surface, has been the subject of extensive research in recent years [1–7]. These types of antennas are highly appealing alternatives to conventional high directivity antennas, including parabolic reflector, phased array, and dielectric lens antennas [8, 9]. Transmitarray antenna is an interesting option to meet the requirements of a lightweight, low-profile, low-cost antenna system for several applications such as satellite-based telecommunications and radars. Transmitarray has a simple structure to be fabricated with common Printed Circuit Board (PCB) technology and its spatial feeding mechanism eliminates the huge insertion loss of a phased array's feeding network, especially at very high frequencies. The transmitarray antenna design process ensures that the transmitted wave phase through the array is in-phase at the normal surface of the main beam desired direction.

A transmitarray antenna could be categorized based on various working principles namely: meta-surfaces [10–12], receive-transmit antenna structure [13–17], and frequency selective surfaces [18–24]. The transmitarrays using receive-transmit antenna structures typically consist of a receiving layer and a transmitting layer that are electrically connected to each other. In Ref. [15], the unit-cell consists of two identical square patch antennas printed on both sides of a substrate. The two layers are connected by a visa. The phase shift of the unit-cell is varied by rotating the relative position of the top layer. Besides, the transmission phase can be changed by varying a phase delay-line. In Ref. [17], a layer of delay lines is inserted between the receiving and the transmitting layer. Tuning the length of the delay lines could be a simple way to control the transmission phase of the unit-cell. However, the size of the unit-cell is relatively large to reserve the space for the delay lines.

Frequency Selective Surface (FSS) is an interesting technique and has been widely used to manipulate electromagnetic fields based on the frequency of the field. It is a type of filter where the filtering is accomplished by the periodic pattern on the surface of the FSS. Traditional FSS are periodic arrays of resonant elements. Each element size is about half-wavelength at frequency of operation. The basic FSS configurations can be represented as low pass, high pass, bandpass or band stop filters. The structures have properties of equivalent inductance and capacitive circuits. By changing the inductance and capacitance, the resonance frequency will be shifted. Therefore, the varied amplitude and phase response of a FSS structure can be created by tuning complex geometries of the resonating element as in Ref. [25–27]. On the other hand, metamaterial Frequency Selective Surfaces (MTM-FSS) operate based on a different principle that allows for many advantages over traditional FSS structures. Instead of using fully resonant unit-cells of traditional FSS, non-resonant unit-cells with much smaller size (typically less than quarter-wavelength)

Manuscript received November 24, 2023; revised February 10, 2024; accepted February 18, 2024; published May 17, 2024.

are used. In non-resonant MTM-FSS, the surface impedance changes very slowly over a wide band. Different works [28, 29] have reported various designs of MTM-FSS with interesting features such as compact size, low sensitivity to oblique incidence angle of the wave.

Clearly, the MTM-FSS structure is more advanced compared to the traditional one. However, traditional FSS structures have their own advantages, such as simplicity in design and manufacturing, ease of frequency response prediction, and suitability for applications where a large FSS is beneficial.

In a typical Multilayer Frequency Selective Surfaces (M-FSS) transmitarray unit-cell the transmission phase is shifted by the field coupling between layers; hence, no phase delay-line is required. This reduces the complexity of a transmitarray design, simplifies the fabrication process and maintains low transmission loss. However, the maximum transmission phase range of a single FSS unit-cell is 90° for −3dB transmission coefficient, as demonstrated in Ref. [30]. To increase the phase range, a large number of layers are employed. In Ref. [5], a unit-cell based on seven layers has been designed to achieve a phase range of 360°. In Ref. [31], five Jerusalem cross patches are printed on five substrates. Due to the large number of layers, FSS-transmitarrays are usually bulky and have large thickness. The number of metallic layers reduced to 3 or 4 has been proposed for unit-cells in Refs. [1, 2, 18, 32]. Each metallic layer is printed on a substrate and the layers are separated by an air gap of $\lambda_0/4$ corresponding to an electrical length of 90°. In Ref. [33], three layers of split diagonal cross patch are printed on three substrates. The use of many substrates leads to the large total thickness while the aperture efficiency ranges from 20% to 35% in most of the mentioned transmitarrays.

In our previous work in Ref. [21], a configuration based on four metallic layers had been proposed for transmitarray unit-cells. The unit-cell design was simple and low profile. Only two dielectric substrates separated by an air gap are used. Simulations and experimental validations of unit-cells confirmed that the combination of C-patches and ring slots could provide a large transmission phase with a low-profile unit-cell structure. The work in Ref. [21] also demonstrated that the phase shift of the unit cell can be controlled by the length of the rectangular slot of the C-slot. With this characteristic, the unit-cell structure allows easy phase tuning without a modification of the Radiating Elements (C-patches) on the top layers. The identical sizes of the radiating elements on the top layers result in constant mutual coupling among adjacent unit cells throughout the array. This ensures that the transmission parameters of a unit cell within the array remain consistent with those of a unit cell simulated using periodic boundary conditions during the design phase. Thanks to the mentioned characteristic, the unit-cell structure can be used to design an electronically reconfigurable transmitarray antenna [34].

To give more information about the C-patch and C-slot characteristics as well as the performance of the proposed unit-cells when they are used to design a transmitarray antenna, in this work, theoretical study on the C-patch and C-slot has been performed and a transmitarray prototype was fabricated and measured.

This paper is organized as follows. In section II, the proposed unit-cell structure is presented. This structure is based on the use of multi-resonance layers, namely C-patches and C-slots. The multi-resonance characteristics of the layers are studied in Section II. (A–B). The effectiveness of the C-patches and C-slots is shown in Section II. C when they are combined to form a M-FSS transmitarray unit-cell. Section III provides an experimental validation for a transmitarray prototype, measured radiation characteristics are reported in this section. Conclusions are drawn in Section IV.

II. Transmitarray Unit-Cell

Our proposed unit-cell is designed using multi-resonant patches on multiple metallic layers. In general, a unit-cell based on multi-layer FSS works as a high order bandpass filter. A higher order of the filter can provide a larger phase range. Therefore, by using a multi-layer FSS with multi-resonant patches on each metallic layer, the unit-cell can obtain a large phase range with low transmission loss and low thickness. In this section, the multi-resonance characteristics of the metallic layers will be analyzed to clarify the characteristics of the whole unit-cell.

A. Design of a C-patch Layer

To understand the resonant characteristics of a FSS layer. The approach in Ref. [35] based on classic transmission-line rules can be used to find the impedance of an arbitrary free-standing FSS layer as follows:

$$Z_{layer} = -\frac{Z_0}{2\Gamma_R}(1+\Gamma_R) \tag{1}$$

where Z_0 is impedance in free space, Γ_R is the reflection coefficient of the layer. By using a full-wave simulation, the reflection coefficient is determined. For each metallic layer, an equivalent circuit model is presented. To simplify the circuit model, ohmic loss is neglected, the impedance of a metallic layer is a pure reactance so that the equivalent circuits are composed of only inductors and capacitors.

The C-patch is a modification of the circular ring patch, the ring element has been widely used in FSS structures [36, 37]. However, the circular ring has single-resonance characteristics, as in Fig. 1(a), the single resonant frequency is at 19.3 GHz, which is far from our desired frequency band. Whereas, with the same size, we can achieve two resonant frequencies when the circular ring is cut with a rectangular gap and shaped into a C-patch.

Fig. 1(b) shows that the impedance of the free-standing C-patch (d_1 = 8.5 mm, d_2 = 1.5 mm, g_1 = 0.6 mm) has two resonant frequencies in the band from 1 GHz to 20 GHz, corresponding to a zero at 10 GHz and a pole at 13 GHz. The equivalent circuit model is derived based on the number of poles and zeros of the layer's impedance. The values of lumped components are determined by fitting the reflection coefficient of the circuit model and reflection coefficient obtained by full-wave simulation. For the

mentioned C-patch and C-slot dimensions, the computed lumped components are L_1 = 28.8 nH, L_2 = 6.92 nH, C_1 = 8.34 fF, C_2 = 8.66 fF.

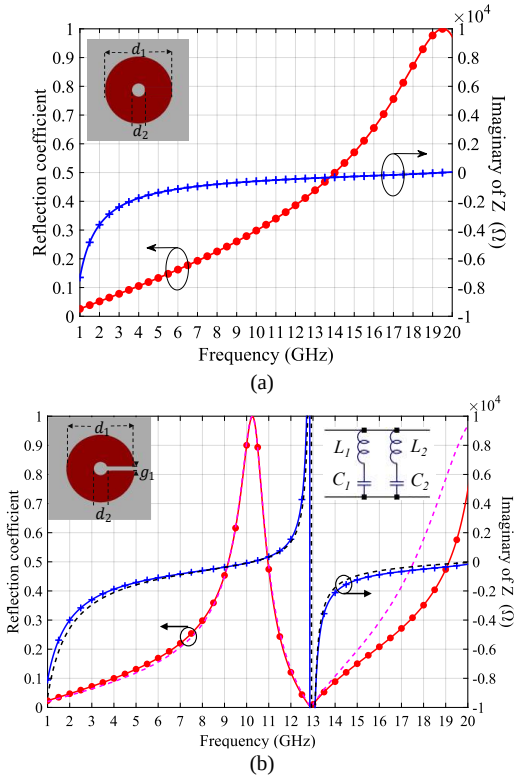

Fig. 1. Impedance and reflection coefficients of a simple circular ring patch (a) and a C-patch (b) that obtained by full-wave simulation (solid curves) and equivalent circuit model (dash curves). (d_1 = 8.5 mm, d_2 = 1.5 mm, g_1 = 0.6 mm)

As can be seen, the reflection coefficients of the equivalent circuit models match to the simulated reflection coefficients. Since the number of LC pairs is proportional to the number of poles and zeros, the equivalent circuits verify the multi-resonance properties of the C-patch and C-slot layers.

B. Design of a C-slot Layer

The idea of design of C-slot patch originates from a simple circular ring slot. The C-slot is the combination of a simple circular ring slot loaded with a rectangular slot (d_3, d_4 are respectively outer and inner diameter of the ring slot and l is the length from the center point of the ring slot to the terminated position of the rectangular slot). As shown in the case when l = 4 mm, (the length of the rectangular slot is minimum) the C-slot becomes a simple circular ring slot. In this case, the ring slot has a single resonant point within 1 GHz to 20 GHz and hence, it does not exhibit multi-resonance characteristic, the second resonance cannot be seen in the frequency range up to 20 GHz. The impedance of the circular ring is characterized by a parallel LC tank. When a rectangular slot is added, the C-slot layer with multi-resonance characteristics can be realized. It is equivalent to a circuit of a series LC (L_3 and C_3) in parallel with a LC tank (L_4 and C_4). The impedance of the free-standing C-slot (d_3 = 9.8 mm, d_4 = 8.0 mm, g_2 = 0.9 mm, l = 0.2 mm) has two poles at 11 GHz and 19 GHz and a zero at 15 GHz, as shown in Fig. 2(a). The computed lumped components are L_3 = 2.47 nH, L_4 = 0.82 nH, C_3 = 47.1 fF, C_4 = 159.9 fF. It is important to find the dimension which affects the resonant frequency so that it can be used to vary the transmission phase. Fig. 2(b) shows that a small change of parameter l has an impact on the impedance of the C-slot layer. Specifically, as l varies from 0.2 mm to 1.2 mm, the resonant frequencies shift toward the higher frequencies. The first resonance (presented by a pole of Z) is merely shifted from 11 GHz to 12 GHz, whereas the second resonance (presented by a zero of Z) is shifted strongly from 15 GHz to 18 GHz. Numerical tests have shown that values of the series L_3 and C_3 control this second resonance. The increase of the terminated position of the rectangular slot (l) can be physically explained by the decrease of the value of C_3. This causes the second resonance to be shifted to higher frequencies.

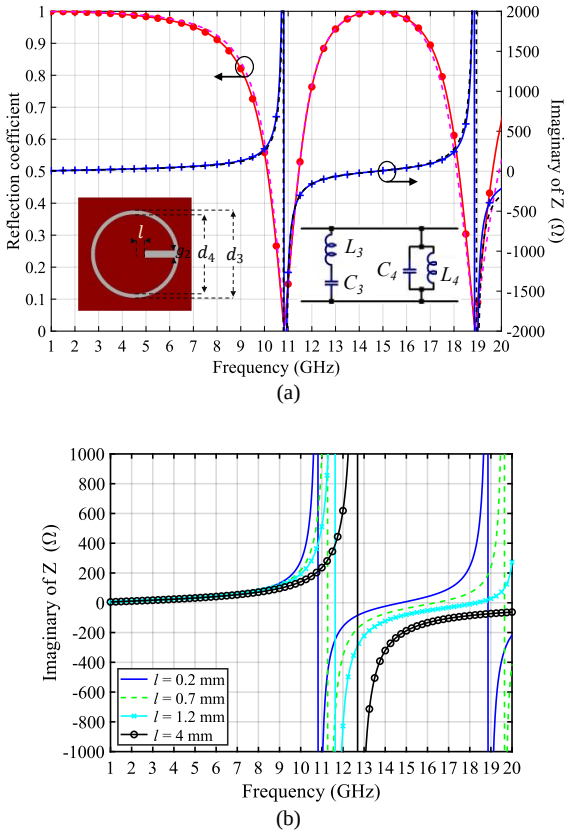

Fig. 2. Multi-resonance characteristic of the C-slot layer. (a) Impedance and reflection coefficients of the C-slot (d_3 = 9.8 mm, d_4 = 8.0 mm, g_2 = 0.9 mm, l = 0.2 mm) obtained by full-wave simulation (solid curves) and equivalent circuit model (dash curves). (b) Resonance shifting due to variation of l.

The interesting point in our design is to use the C-slot, in which the rectangular slot introduces a second resonance in the layer. This resonance is immensely sensitive to the length of the rectangular slot. The resonance is shifted strongly with a small change of the parameter l. A large variation of transmission phase range can be obtained by varying only l in the C-slot layer. This, in turn, reduces the need for tuning other dimensions. Consequently, the unit-cell, formed by combining the C-

patch and C-slot layers, is designed to provide a large phase range, thanks to the presence of multi-resonances.

C. Unit-Cell Design Using Multi-resonant C-patches and C-slots

The unit-cell structure is illustrated in Fig. 3. It is designed using two identical substrates which are Roger 4003C substrates with a thickness $ht = 1.542$ mm and $\varepsilon_r = 3.55$. The two substrates are stacked on top of each other and separated by a 1.5 mm layer of air. For each substrate, a C-patch is printed on the top while a C-slot is printed on the bottom. The structure operates with a linear polarization. In this case, the orientation of E-field is perpendicular to the gap of the C-patch, as depicted in Fig. 3. Table I shows detailed dimensions of the four unit-cells. Total thickness of a unit-cell is 4.584 mm corresponding to $0.18\lambda_0$ and the cell size equals $0.54\lambda_0$, where λ_0 is the wavelength in free-space.

TABLE I. DIMENSIONS OF THE FOUR UNIT-CELLS

Unit-cell	Layer 1&4		Layer 2&3		
	d_1	d_2	d_3	d_4	l
UC1	9	1.8	10.8	9.8	0
UC2	8.5	1.8	9.8	8	0.2
UC3	8.5	1.8	9.8	8	1.2
UC4	8.5	1.8	9.8	8	1.7

$g_1 = 0.6; g_2 = 0.9; p = 14; s = 1.5; ht = 1.542$. Unit: mm

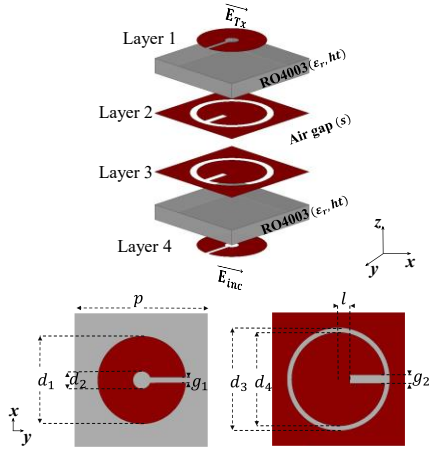

Fig. 3. Geometry of the proposed unit-cell structure.

The full equivalent circuit model of this quad-layer configuration can be constructed based on the combination of the equivalent circuit model of each layer as presented in [21]. In our unit-cell structure, the equivalent circuit has seven cascaded sections including four conductor layers, two dielectric substrates and an air gap. Each dielectric substrate is equivalent to a short transmission line, as studied in [38], which can be represented by a as series inductor $Lt = ht \times \mu_0\mu_r$ and a shunt capacitor $Ct = (\varepsilon_0\varepsilon_r \times ht)/2$. Where μ_0, ε_0 are permeability and permittivity of free space, respectively. μ_r, ε_r are relative permeability and permittivity of the dielectric substrate and ht is the substrate thickness. The substrate thickness has a direct impact to Lt, which affects the coupling between the resonance of the C-patch and C-slot layer. With an appropriate thickness, the transmission magnitude can be enhanced to provide pass-band behavior. On the other hand, the capacitance values in the circuit model of C-patch and C-slot layers are modified when the permittivity varies. For this reason, variation of dieletric permittivity will have an impact on shifting the resonant frequencies of the unit-cell structure.

For UC2, UC3 and UC4, the transmission phase is changed by varying the length of the rectangular slots in the middle layers with a step of 0.5 mm. As mentioned, the second resonant frequency varies with a large range when l varies from 0.2 mm to 1.7 mm. This allows UC2 and UC4 to have a large phase shift of about 200° at 11.5 GHz, as shown in Fig. 4(b). Further increasing of l will cause the resonant frequency to shift further to higher frequencies. However, this also means that at frequencies below 11.2 GHz, the phase curves cannot be as linear as those at higher frequencies. The phase variation is small even with a larger value of l. That is due to the small change of the first resonant frequency when L_3 and C_3 changes, whereas the first resonance is mainly controlled by the parallel L_4 and C_4. In order to get the fourth phase state, UC1 is optimized by a small change of the C-patch and C-slot.

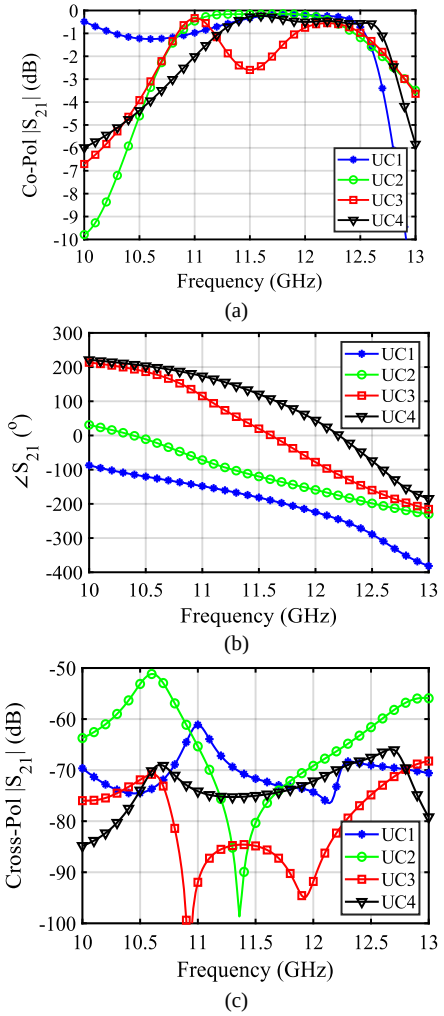

Fig. 4. Simulated transmission coefficients of the four unit-cells. (a) co-polarized transmission magnitude, (b) transmission phase and (c) cross-polarized transmission magnitude.

The unit-cell structure has been simulated by using ANSYS HFSS software, version 15. The unit-cell is simulated under array environment by using two Floquet ports and Master-Slave boundaries, with a normal incident wave. The simulated transmission phase and magnitude of four phase states are shown in Fig. 4. As can be seen, two adjacent phase states are separated by circa 90° at –11.8 GHz. The four unit-cells cover a large common 3 dB transmission bandwidth, from 10.8 GHz to 12.7 GHz, corresponding to 16.1% fractional bandwidth. The transmission magnitude is better than –1.5 dB at 11.8 GHz. The cross-transmission coefficients of the unit-cells are shown in Fig. 4(c). They remain under –50 dB for all states.

III. Transmitarray Antenna Validation

A. Transmitarray Design Based on 2-bit Phase Resolution Unit-Cells

In the context of the beam focusing transmitarray, the individual unit-cells are designed to intercept the incoming wave that is emitted from the feed horn. Upon receiving this signal, these unit-cells are then responsible for re-transmitting the signal. It is crucial that this transmission maintains a uniform phase across the entire aperture of the transmitarray.

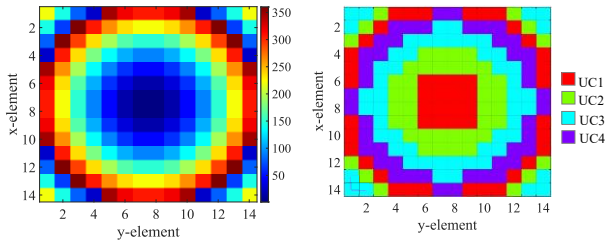

(a) (b)

Fig. 5. Phase distribution in the transmitarray aperture (a) Ideal phase, (b) Quantized phase.

To focus the beam at a specific direction (θ, ϕ), the required phase distribution across the transmitarray aperture is first calculated by Eq. (2) and then a phase quantization process in Eq. (4) transforms the ideal phase into the closest phase that the unit-cell can provide. The phase distribution is shown in Fig. 5.

$$\varphi(x_i, y_i) = k_0\left(r_i - sin\theta(x_i cos\phi + y_i sin\phi)\right) \quad (2)$$

$$r_i = \sqrt{x_i^2 + y_i^2 + F^2} \quad (3)$$

$$\psi(x_i, y_i) = \begin{cases} \text{UC1} & -45^\circ < \varphi(x_i, y_i) < 45^\circ \\ \text{UC2} & 45^\circ \le \varphi(x_i, y_i) < 135^\circ \\ \text{UC3} & 135^\circ \le \varphi(x_i, y_i) \le 225^\circ \\ \text{UC4} & 225^\circ \le \varphi(x_i, y_i) \le 315^\circ \end{cases} \quad (4)$$

where k_0 is propagation constant, $\varphi(x_i, y_i)$ is required phase at i^{th} unit-cell with position x_i, y_i. F is focal length.

B. Measurement of a Transmitarray Prototype

Fig. 6 shows a transmitarray antenna prototype which has been fabricated and measured in an anechoic chamber. The transmitarray includes 196 unit-cells arranged in a 14-by-14 square lattice. As the unit-cell size is 14 × 14 × 4.58 mm^3, the total size of the transmitarray is $7.7\lambda_0 \times 7.7\lambda_0 \times 0.18\lambda_0$ at 11.8 GHz. The feed source is a small pyramidal horn antenna customized for nominal gain of 10 dBi, the aperture of the horn is 23×32 mm^2. The 10-dB beamwidths of both E-plane and H-plane have no considerable difference in our testing frequency range. At 11.8 GHz, its gain is 10.4 dBi, and its E-plane and H-plane 10-dB beamwidths are approximately 100° and 110°, respectively. The feed source is placed at a focal point of 175 mm away from the transmitarray, corresponding to a -8 dB edge illumination of the feed horn. To create an air gap between the two substrates of the transmitarray, a hollow acrylic frame is attached between two substrates. It has a thickness of 1.5 mm. It also plays a role as an extended frame to fix the array in four supporting columns.

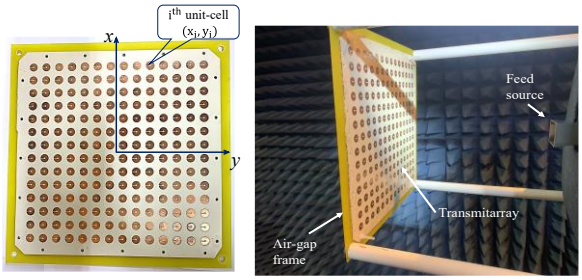

(a) (b)

Fig. 6. Fabricated transmitarray prototype, (a) A transmitarray prototype consisting of 196 unit-cells and (b) measurement setup in anechoic chamber.

The transmitarray is measured by NSI near-field measurement system in which the distance between the transmitter antenna to the transmitarray-under-test is 268 mm. In the range of 10 GHz to 12 GHz, this distance is within the near-field distance of the transmitarray-under-test. Far-field radiation characteristics are finally extracted by a Near-field-to-Far-field transformation built-in software.

The normalized radiation patterns of the prototype transmitarray are simulated and measured, as presented in Fig. 7. The pencil beam is successfully formed at broadside direction $(\theta = 0°, \phi = 0°)$. The co-pol patterns of the main lobe are almost superimposed in both simulated and measured results. The side lobe level is below 18 dB in both cut planes. As depicted by measured cross-pol radiation patterns, the polarization purity is very good, providing an isolation of around 30 dB between co-polarizations and cross-polarizations.

At the focal length of 175 mm, the gain of the transmitarray reaches maximum of 25 dBi at 11.8 GHz, corresponding to the aperture efficiency of 43%. The 1-dB and 2-dB gain bandwidth are 7% and 11%, respectively.

Table II shows a comparison between the proposed transmitarray designs and other existing designs. Our transmitarray is highlighted with the high aperture efficiency and has a much lower thickness compared to other transmitarray designs. Furthermore, our design uses only two substrates, making the transmitarray not only cost-effective but also simple to fabricate and install.

TABLE II. COMPARISION BETWEEN THE PROPOSED TRANSMITARRAY WITH OTHER EXISTING DESIGNS

Ref.	Freq. [GHz]	Number of layers	Number of substrates	Total thickness	Aperture efficiency	Gain bandwidth (1–dB/ 3–dB)
[2]	11.3	3	2	$0.51\lambda_0$	30%	9% / 17.7%
[18]	30	4	4	$0.95\lambda_0$	47%	7.5% / -
[31]	12	5	5	$0.58\lambda_0$	34.6%	10% / -
[33]	12.5	3	3	$0.52\lambda_0$	20.9%	9.6% / -
[39]	19	4	3	$0.69\lambda_0$	34.9%	18% / >25.5%
This work	**11.5**	**4**	**2**	**$0.18\lambda_0$**	**43%**	**7% / -**

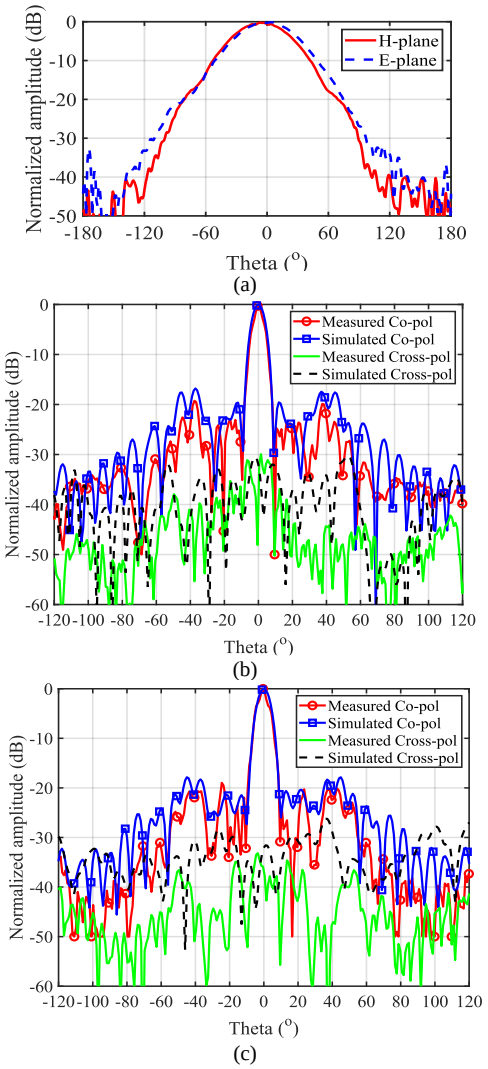

Fig. 7. Radiation patterns at 11.8 GHz of the feed horn antenna (a), radiation patterns of the transmitarray in H-plane (b) and E-plane (c).

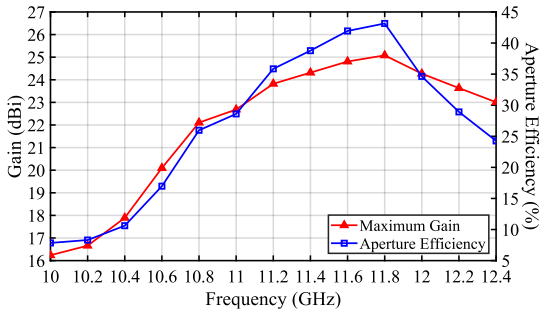

Fig. 8. Measured peak gain and corresponding aperture efficiency of the transmitarray.

IV. CONCLUSION

This paper has presented the use of multi-resonance C-patch and C-slot to design a transmitarray unit-cell structure. The unit-cell was designed to provide four different phase states with a large phase range, wide -3 dB transmission bandwidth. A 196-element transmitarray prototype has been characterized. Measured results confirm that transmitarray using the proposed unit-cell structure has good radiation characteristics and high aperture efficiency. It is worth to emphasize that the key attribute of our transmitarray unit-cell structure is the ease of phase tuning just by varying the length of the rectangular slot in the C-slot layers. In our vision, this unit-cell structure has a great potential in a design of an electronically reconfigurable transmitarray where switching devices (p-i-n diodes, RF-MEMS) can be inserted at different positions along the rectangular slot of the C-slots to control the slot length, consequently the transmission phase shift. As a result, this unit-cell structure has several advantages such as design simplicity, low thickness, cost-effectiveness and capability of electronically reconfigurable unit-cells.

CONFLICT OF INTEREST

The authors declare no conflict of interest.

AUTHOR CONTRIBUTIONS

M.T.N. conducted the research, conducted the measurement, analyzed the data, and wrote the paper; L.M. carried out the research, performed the measurement, examined the data, and prepared the paper; B.D.N. conducted the research, carried out the measurement, analyzed the data, and composed the paper; all authors had approved the final version.

FUNDING

This research is funded by the Vietnam National University HoChiMinh City (VNU-HCM) under grant number C2022-28-05.

REFERENCES

[1] G. Liu, H. J. Wang, J. S. Jiang, F. Xue, and M. Yi, "A high-efficiency transmitarray antenna using double split ring slot elements," *IEEE Antennas Wirel Propag Lett*, vol. 14, pp. 1415–1418, 2015.

[2] A. H. Abdelrahman, A. Z. Elsherbeni, and F. Yang, "High-gain and broadband transmitarray antenna using triple-layer spiral dipole elements," *IEEE Antennas Wirel Propag Lett*, vol. 13, pp. 1288–1291, 2014.
[3] Y. L. Zhang, X. Z. Lv, J. X. Han, S. Bao, Y. Cai, and Z. Wu, "A highly efficient dual-band transmitarray antenna using cross and square rings elements," *Applied Computational Electromagnetics Society Journal (ACES)*, vol. 36, no. 07, pp. 852–857, Oct. 2021.
[4] E. B. Lima, S. A. Matos, J. R. Costa, C. A. Fernandes, and N. J. G. Fonseca, "Circular polarization wide-angle beam steering at ka-band by in-plane translation of a plate lens antenna," *IEEE Trans Antennas Propag*, vol. 63, no. 12, pp. 5443–5455, Dec. 2015.
[5] J. G. Nicholls and S. V. Hum, "Full-space electronic beam-steering transmitarray with integrated leaky-wave feed," *IEEE Trans Antennas Propag*, vol. 64, no. 8, pp. 3410–3422, Aug. 2016.
[6] L. D. Palma, A. Clemente, L. Dussopt, R. Sauleau, P. Potier, and P. Pouliguen, "Circularly-polarized reconfigurable transmitarray in ka-band with beam scanning and polarization switching capabilities," *IEEE Trans Antennas Propag*, vol. 65, no. 2, pp. 529–540, Feb. 2017.
[7] K. Pham *et al.*, "Design of wideband dual linearly polarized transmitarray antennas," *IEEE Trans Antennas Propag*, vol. 64, no. 5, pp. 2022–2026, May 2016.
[8] P. Bia, D. Caratelli, L. Mescia, and J. Gielis, "Analysis and synthesis of supershaped dielectric lens antennas," *IET Microwaves, Antennas & Propagation*, vol. 9, no. 14, pp. 1497–1504, Nov. 2015.
[9] A. Belen and E. Tetik, "Realization of modified elliptical shaped dielectric lens antenna for X band applications with 3D printing technology," *The Applied Computational Electromagnetics Society Journal (ACES)*, vol. 35, no. 8, pp. 916–921, Aug. 2020.
[10] M. Jiang, Z. N. Chen, Y. Zhang, W. Hong, and X. Xuan, "Metamaterial-based thin planar lens antenna for spatial beamforming and multibeam massive MIMO," *IEEE Trans Antennas Propag*, vol. 65, no. 2, pp. 464–472, Feb. 2017.
[11] Y. Liu, A. Zhang, Z. Xu, S. Xia, and H. Shi, "Wideband and low-profile transmitarray antenna using transmissive metasurface," *J Appl Phys*, vol. 125, no. 4, Jan. 2019.
[12] H. Li, G. Wang, H. X. Xu, T. Cai, and J. Liang, "X-band phase-gradient metasurface for high-gain lens antenna application," *IEEE Trans Antennas Propag*, vol. 63, no. 11, pp. 5144–5149, Nov. 2015.
[13] W. An, S. Xu, F. Yang, and M. Li, "A double-layer transmitarray antenna using malta crosses with vias," *IEEE Trans Antennas Propag*, vol. 64, no. 3, pp. 1120–1125, Mar. 2016.
[14] K. T. Pham, R. Sauleau, E. Fourn, F. Diaby, A. Clemente, and L. Dussopt, "Dual-band transmitarrays with dual-linear polarization at ka-band," *IEEE Trans Antennas Propag*, vol. 65, no. 12, pp. 7009–7018, Dec. 2017.
[15] H. Kaouach, L. Dussopt, J. Lanteri, T. Koleck, and R. Sauleau, "Wideband low-loss linear and circular polarization transmit-arrays in V-Band," *IEEE Trans Antennas Propag*, vol. 59, no. 7, pp. 2513–2523, Jul. 2011.
[16] D. M. Pozar, "Flat lens antenna concept using aperture coupled microstrip patches," *Electron Lett*, vol. 32, no. 23, pp. 2109–2111, 1996.
[17] Y. M. Cai *et al.*, "A novel ultrawideband transmitarray design using tightly coupled dipole elements," *IEEE Trans Antennas Propag*, vol. 67, no. 1, pp. 242–250, Jan. 2019.
[18] C. G. M. Ryan, M. R. Chaharmir, J. Shaker, J. R. Bray, Y. M. M. Antar, and A. Ittipiboon, "A wideband transmitarray using dual-resonant double square rings," *IEEE Trans Antennas Propag*, vol. 58, no. 5, pp. 1486–1493, May 2010.
[19] J. R. Reis *et al.*, "FSS-Inspired transmitarray for two-dimensional antenna beamsteering," *IEEE Trans Antennas Propag*, vol. 64, no. 6, pp. 2197–2206, Jun. 2016.
[20] M. Thien Nguyen and B. D. Nguyen, "Wideband unit-cell design for X-band transmitarray," in *Proc. ANTEM 2018: 2018 18th International Symposium on Antenna Technology and Applied Electromagnetics*, vol. 1, 2018.
[21] B. D. Nguyen and M. T. Nguyen, "Three-bit unit-cell with low profile for X-band linearly polarized transmitarrays," *The Applied Computational Electromagnetics Society Journal (ACES)*, vol. 34, no. 9, pp. 1334–1339, Sep. 2019.
[22] P. Mei, G. F. Pedersen, and S. Zhang, "A broadband and FSS-based Transmitarray antenna for 5G millimeter-wave applications," *IEEE Antennas Wirel Propag Lett*, vol. 20, no. 1, pp. 103–107, Jan. 2021.
[23] M. T. Nguyen, T. T. Nguyen, and B. D. Nguyen, "Wideband transmitarray unit-cell design with 1-Bit phase control and twistable polarization," *IEEE Microwave and Wireless Components Letters*, vol. 32, no. 6, pp. 627–630, Jun. 2022.
[24] M. T. Nguyen and B. D. Nguyen, "Low thickness transmitarray unit-cell for wideband millimeter-wave applications," in *Proc. IEEE Conference on Antenna Measurements and Applications, CAMA*, Guangzhou, Dec. 2022.
[25] B. A. Munk, *Frequency Selective Surfaces*, Wiley, 2000.
[26] I. Ullah, "Measuring and filtering microwave radiations using frequency selective surface through energy saving glass," Edith Cowan University, 2012.
[27] C. Caloz and T. Itoh, *Electromagnetic Metamaterials: Transmission Line Theory and Microwave Applications*. 2005. Accessed: Feb. 05, 2024.
[28] S. Narayan, G. Gulati, B. Sangeetha, and R. U. Nair, "Novel metamaterial-element-based FSS for airborne radome applications," *IEEE Trans Antennas Propag*, vol. 66, no. 9, pp. 4695–4707, Sep. 2018.
[29] S. Gu, B. Su, and X. Zhao, "Planar isotropic broadband metamaterial absorber," *J Appl Phys*, vol. 114, no. 16, Oct. 2013.
[30] A. H. Abdelrahman, A. Z. Elsherbeni, and F. Yang, "Transmission phase limit of multilayer frequency-selective surfaces for transmitarray designs," *IEEE Trans Antennas Propag*, vol. 62, no. 2, pp. 690–697, 2014.
[31] M. N. Jazi, M. R. Chaharmir, J. Shaker, and A. R. Sebak, "Broadband transmitarray antenna design using polarization-insensitive frequency selective surfaces," *IEEE Trans Antennas Propag*, vol. 64, no. 1, pp. 99–108, Jan. 2016.
[32] C. Tian, Y. C. Jiao, G. Zhao, and H. Wang, "A wideband transmitarray using triple-layer elements combined with cross slots and double square rings," *IEEE Antennas Wirel Propag Lett*, vol. 16, pp. 1561–1564, 2017.
[33] J. Yu, L. Chen, J. Yang, and X. Shi, "Design of a transmitarray using split diagonal cross elements with limited phase range," *IEEE Antennas Wirel Propag Lett*, vol. 15, pp. 1514–1517, 2016.
[34] B. D. Nguyen and C. Pichot, "Unit-cell loaded with PIN diodes for 1-Bit linearly polarized reconfigurable transmitarrays," *IEEE Antennas Wirel Propag Lett*, vol. 18, no. 1, pp. 98–102, Jan. 2019.
[35] F. Costa, A. Monorchio, and G. Manara, "Efficient analysis of frequency-selective surfaces by a simple equivalent-circuit model," *IEEE Antennas Propag Mag*, vol. 54, no. 4, pp. 35–48, 2012.
[36] X. Yao, M. Bai, and J. Miao, "Equivalent circuit method for analyzing frequency selective surface with ring patch in oblique angles of incidence," *IEEE Antennas Wirel Propag Lett*, vol. 10, pp. 820–823, 2011.
[37] A. A. Dewani, S. G. O'Keefe, D. V. Thiel, and A. Galehdar, "Optically transparent frequency selective surfaces on flexible thin plastic substrates," *AIP Adv*, vol. 5, no. 2, p. 27107, Feb. 2015.
[38] M. Al-Joumayly and N. Behdad, "A new technique for design of low-profile, second-order, bandpass frequency selective surfaces," *IEEE Trans Antennas Propag*, vol. 57, no. 2, pp. 452–459, Feb. 2009.
[39] H. Nematollahi, J. J. Laurin, M. Barba, and J. A. Encinar, "Realization of focused beam and shaped beam transmitarrays based on broadband unit cells," *IEEE Trans Antennas Propag*, vol. 65, no. 8, pp. 4368–4373, Aug. 2017.